COMMUNICATIONS IN SCIENCE AND TECHNOLOGY
Homepage: cst.kipmi.or.id

Photocatalytic degradation of methylene blue and Congo red dyes from aqueous solutions by bentonite-Fe_3O_4 magnetic

Fahma Riyanti[a,b], Hasanudin Hasanudin[b], Addy Rachmat[b], Widia Purwaningrum,[a,b], Poedji Loekitowati Hariani[b,*]

[a]*Doctoral Program of Mathematics and Natural Sciences, Faculty of Mathematics and Natural Sciences, Universitas Sriwijaya, Palembang 30139, Indonesia*
[b]*Research Group on Magnetic Materials, Department of Chemistry, Faculty of Mathematics and Natural Sciences, Universitas Sriwijaya, Ogan Ilir 30662, Indonesia*

Article history:
Received: 15 October 2022 / Received in revised form: 28 January 2023 / Accepted: 16 February 2023

Abstract

This study describes the co-precipitation synthesis of magnetic bentonite-Fe_3O_4 for photocatalytic degradation of methylene blue and Congo red pigments under visible light. Bentonite-Fe3O4 composites were produced using the mass ratio of 2:1 and 1:1 for bentonite to Fe3O4, respectively. X-ray Powder Diffraction (XRD), Fourier Transform Infra-Red (FTIR), BET surface area, Vibrating-Sample Magnetometer (VSM), Scanning Electron Microscopy with Energy Dispersive Spectroscopy (SEM-EDS), and Ultraviolet–Visible Diffuse Reflectance Spectroscopy (UV DRS) were used to characterize the materials. The bentonite-Fe3O4 (1:1) composite exhibited a greater surface area in comparison to the bentonite-Fe3O4 (2:1) composite with a measured value of 106.6 m2/g. It is a superparamagnetic material with a band gap of 2.25 eV and a saturation magnetization of 69.64 emu/g. The photocatalytic degradation of dye using bentonite-Fe3O4 (1:1) with the initial dye concentration of 25 mg/L, volume of 50 mL, catalyst dose of 0.05 g/L, addition of 3 mL H_2O_2, and 90 minutes of visible irradiation resulted in 94.34% and 98.45% degradation efficiency of methylene blue and Congo red dyes, respectively. The study determined that the most favorable pH for the photocatalytic degradation of methylene blue was pH 11, whereas the optimal pH for Congo red was found at pH 5. For methylene blue and Congo red dyes, photocatalytic degradation followed pseudo-first-order with the constant rates of 0.0356 min-1 and 0.0348 min-1, respectively. After five cycles of use in the photocatalytic process, the catalyst's degradation efficiency fell into below 5%. This research demonstrated that catalysts could be utilized in wastewater treatment technology.

Keywords: bentonite-Fe_3O_4; magnetic; degradation photocatalytic; methylene blue, Congo red

1. Introduction

Environmental pollution is a significant problem, and one of the pollutants of concern is dyes. Industries whose processes produce waste containing dyes include the textile, leather, food, cosmetic, paper, pharmaceutical, plastic, and dye product industries [1,2]. Liquid waste from industries using high dyes significantly impacts aquatic ecosystems and human health [3, 4]. Wastewater containing dyes can cause water problems, including high chemical oxygen demand (COD), reduced light penetration, reduced oxygen concentration in waters, and mutagenic or carcinogenic effects [5,6]. More than 100 types of commercial dyes are available and 7.10^5 tonnes of dyes are produced. Since the most of dyes are disposed of as waste [7], it is of utmost significance to minimize the dye levels in industrial wastewater prior to its release into the ecosystem.

Various technologies have been employed to reduce the concentration of the dye, such as adsorption [4], coagulation-flocculation [8], electrochemical oxidation [9], membrane separation [10], ozonation [11], and photocatalytic degradation [12]. Photocatalytic degradation here becomes a promising method to manage this problem as it can oxidize harmful organic and inorganic pollutants [13,14]. Upon the energy absorption, the photocatalyst undergoes the excitation of electrons from the valence bond (VB) to the conduction band (CB). The process results in vacancies in the VB (h^+) and photoinduced electrons in the CB (e^-). During the entirety of the reaction process, the photocatalyst remains unaltered. The VB holes indicate a potent oxidation capability, while the conducting electron acts as a reducing agent. [15].

Spinel ferrite is denoted by MFe_2O_4 where M signifies the metal cation. It can exhibit magnetic properties that can be used for many applications [16,17]. Ferrite is an n-type semiconductor with exceptional magnetic properties and chemical stability. It has a band gap less than or equal to 2 eV and becomes efficacious under visible light irradiation [18,19]. Spinel structure increases photocatalytic efficiency because the active catalyst site is located in the crystal lattice [20]. TiO_2 and ZnO are semiconductors often used for photocatalysts with band gap > 3.0 eV [21]. The drawback is that they primarily absorb UV light less than 4% absorption occurred in the visible

* Corresponding author.
Email: puji_lukitowati@mipa.unsri.ac.id
https://doi.org/10.21924/cst.8.1.2023.1007

region. TiO_2 or ZnO undergoes fast recombining photo-generated holes and electrons during photocatalytic degradation [22,23]. Therefore, it is relevant to develop catalysts capable of absorbing visible light. After photocatalytic degradation, ferrite compounds, due to their magnetic properties, can be separated from the solution using permanent magnets. Several ferrite compounds have been used for photocatalytic degradation [24], Fe_3O_4 for the degradation of naphthalene [25], $ZnFe_2O_4$ for the degradation of green malachite and rhodamine B [22] and $CoFe_2O_4$ for the methylene blue dye degradation [19].

Fe_3O_4 (magnetite) is a ferrite compound used as a heterogeneous catalyst for having high magnetic properties, and being stable, low-cost, and environmentally friendly [26]. Some its disadvantages are that it is easy to agglomerate and unstable under acidic conditions [27]. To avoid agglomeration, some studies combined it with several materials, such as chitosan [28], magnetic graphene oxide-biomass activated carbon [29], and Fe_3O_4/PVA [30]. Meanwhile, bentonite is widely used for catalytic support [31]; it has a potential to be combined with Fe_3O_4 because of its excellent adsorption properties, interlayer space on the surface, low cost, chemical and mechanical stability, and great abundance [32-33]. Bentonite can protect Fe_3O_4 from agglomeration, oxidation, and the stability of Fe_3O_4 in acidic media [34]. Previous research indicated that bentonite possesses a band gap exceeding 3 eV. The introduction of MnO_2 onto bentonite results in a reduction of the band gap by approximately 2 eV, thereby enabling the absorption of visible light irradiation [30].

The catalyst is combined with an oxidizing agent, such as H_2O_2 to increase the degradation efficiency. The addition of H_2O_2 increases the number of hydroxyl radicals in the dyes' degradation [19]. Another study showed that the photocatalytic degradation combination using $NiFe_2O_4$ and H_2O_2 increased the Congo red dye degradation efficiency compared to $NiFe_2O_4$ [23], and the photocatalytic efficiency of methylene blue dye using Fe_3O_4 + H_2O_2 was more significant than Fe_3O_4 [35].

In this study, the co-precipitation method was utilized to synthesize bentonite-Fe3O4 magnetic. The product was employed for the photocatalytic degradation of synthetic dyes. The effects of pH solution, initial dye concentration, H_2O_2 volume, and irradiation time were studied as well.

2. Materials and Methods

2.1. Materials

Chemicals, including Iron(III) chloride hexahydrate ($FeCl_3.6H_2O$), Iron(II) chloride tetrahydrate ($FeCl_2.4H_2O$), hydrogen peroxide (H_2O_2), hydrochloric acid (HCl), sodium hydroxide (NaOH), methylene blue ($C_{16}H_{18}ClN_3S$) and Congo red ($C_{32}H_{22}N_6Na_2O_6S_2$), sodium chloride (NaCl) were procured from Sigma-Aldrich, United States and were of high purity. Meanwhile, natural bentonite was obtained from Sorolangun, Jambi.

2.2. Bentonite preparations

The natural bentonite was dried in an oven at 105ºC for 10 hours. The substance underwent grinding via a mortar and subsequent sieving through a 200 mesh. The powder was soaked in 1%HCl solution for 4 hours at room temperature and washed using deionized water until reaching the neutral pH. Meanwhile, bentonite was dried in an oven at 105ºC for 2 hours.

2.3. Synthesis of bentonite-Fe_3O_4

The composite with a mass ratio of bentonite: Fe_3O_4 = 1:1 was prepared as follows. 25 mL deionized water containing 1.72 g $FeCl_2 \cdot 4H_2O$, and 4.67 g $FeCl_3 \cdot 6H_2O$, 2.0 g bentonite was added. The resulting mixture was agitated with a magnetic stirrer and heated to a temperature of 60ºC. A 1 M NaOH solution was gradually added to the solution while stirring at 100 rpm for about one hour until the pH reached approximately 10. Permanent magnets were employed to separate the black precipitate (bentonite-Fe3O4) from the solution. The precipitate underwent neutralization with distilled water and subsequently was dried in an oven at 105ºC for 1 hour. Bentonite-Fe_3O_4 (2:1) was prepared through a similar method using bentonite mass 4.0 g.

2.4. Characterization

Various instruments were utilized to characterize bentonite, bentonite-Fe_3O_4 (2:1), and bentonite-Fe_3O_4 (1:1). Structural characterization was conducted using X-ray diffraction (XRD PANalytical) with Cu-Kα radiation (λ=1.5418Å), range 2θ = 5-80º at the scan rate of 0.03º min^{-1}. Functional groups were determined using Fourier Transform Infrared (FTIR Prestige 21 Shimadzu) at wave numbers 400-4000 cm^{-1}. Meanwhile, a scanning Electron Microscope-Energy Dispersive Spectrometer (SEM-EDS JOEL JSM 6510 LA) was used to determine the morphology and element composition. The magnetic properties were analyzed using a Vibrating Sample Magnetometer (VSM Oxford Type 1.2 T), while the surface area and pore size analyzer were investigated using N_2 adsorption-desorption (Quantachrome NOVa Touch 4LX). Band gaps were explored using Ultraviolet–Visible Diffuse Reflectance Spectroscopy (UV-Vis DRS Pharmaspec UV-1700). The band gap value was determined using Eq. (1) [19]:

$$(\alpha hv)^n = A(hv - Eg)^n \quad (1)$$

where α is the absorption coefficient, hv is the photon energy, A is the optical constant, and Eg is the optical energy band gap. n can take on a value of either 2 or ½ in the direct and indirect transitions. The TOC analyzer (TOC Teledyne Tekmar) was utilized to determine the total organic carbon. The UV-Vis Spectrophotometer (Type Orion Aquamate 8000) was utilized to measure the absorbance of the dye.

2.5. Point of zero charges (pHpzc) determination

A catalyst of 0.15 g was added to 25 mL of 0.1 M NaCl solution. The pH was adjusted to 2-12 using 0.1 M HCl and 0.1 M NaOH. The solution was agitated with a shaker for 2 hours and subsequently allowed to rest for 24 hours. The pH meter ascertained the initial and final pH and the pHpzc was ascertained by analyzing the initial pH curve vs. ΔpH.

2.4. Photocatalytic Degradation

The experiment was carried out using the batch method. A 50 mL of dye (methylene blue/Congo red) with a concentration of 25 mg/L was added to 0.05 g/L bentonite-Fe_3O_4 (1:1) and pH was adjusted between 3 and 12 using HCl and NaOH 0.1 M solution. The mixture was put into a photoreactor and irradiated with visible light at a distance of ± 30 cm from the light source (60 watts, Phillip lamps). Before photocatalytic degradation, the solution was stirred using a magnetic stirrer for 30 minutes in the dark to obtain adsorption-desorption equilibrium degradation. The photocatalytic degradation variables included the initial dye concentration of 25, 50, 75, 100, 125, and 150 mg/L, H_2O_2 addition was 1, 2, 3, 4, and 5 mL, and the irradiation time was for 10-120 minutes. The degradation efficiency (%) was calculated using Eq. (2):

$$\text{Degradation } (\%) = \frac{C_o - C_t}{C_o} \quad (2)$$

where C_o and C_t refer to initial and final concentrations of dye (mg/L).

The reusability was determined by washing the catalyst for the photocatalytic degradation process at optimum conditions using deionized water and ethanol three times. The sample was subjected to drying in an oven at 70°C for 3 hours and subsequently reused for photocatalytic degradation. The same experiment was repeated up to 5 times [25].

3. Results and Discussion

3.1. Characteristics of Bentonite, Bentonite-Fe_3O_4 (2:1), and Bentonite-Fe_3O_4 (1:1)

Figure 1 presents the XRD spectra of bentonite and the composites. The characteristics peaks of bentonite in the sharp peaks form were observed at 2θ = 20.86º, 26.66º, 36.54º and 54.94º, which were planes (110), (210), (124) and (144) according to the standard of JCPDS bentonite (No. 01-088-0891). The peak with high intensity at 26.66º with d (Å) of 3.33 was the SiO_2 of the Quartz phase according to JCPDS No. 46-1045. In contrast, the bentonite-Fe_3O_4 peak had a lower intensity than bentonite with the presence of the new peak at 2θ = 35.78º and 35.67º in bentonite-Fe_3O_4 of 2:1 and 1:1 ratio. The cubic spinel phase of Fe_3O_4 was detected at 2θ around 30°, 35°, 43°, 53°, 57°, and 62º, covering planes (220), (311), (400), (422), (511), and (440) according to JCPDS Fe_3O_4 No. 65-3107.

The Scherrer formula yielded an average crystal size of 18.4 nm for bentonite. Meanwhile, the crystal sizes for bentonite-Fe_3O_4 (2:1) and bentonite-Fe_3O_4 (1:1) were 10.5 and 14.8 nm, respectively. The smaller crystal size of bentonite-Fe_3O_4 compared to bentonite indicated Fe_3O_4 dispersed on the bentonite surface and intercalated into the bentonite layer.

Figure 2 displays the FTIR spectra of bentonite and the composites. The bending vibrations of water absorption, specifically H-O-H and O-H, are represented by wave numbers around 3400 cm^{-1} and 1600 cm^{-1}. The absorption bands appeared in all three spectra. Jiang et al. [34] reported that the spectra at wave numbers close to 3630 cm^{-1} were Si/Al-OH stretching bands. The wave numbers observed were 3620.8 cm^{-1} for bentonite and 3620.2 cm^{-1} for both composites. Si-O-Si stretching bonds were observed at the wave numbers of 1004.8 cm^{-1} in bentonite, while bentonite-Fe_3O_4 (2:1) and bentonite-Fe_3O_4 (1:1) appeared at 1006.7 cm^{-1} and 1004.6 cm^{-1}. The band at 800 cm^{-1} was correlated with Si(Al)-O stretching vibration [36].

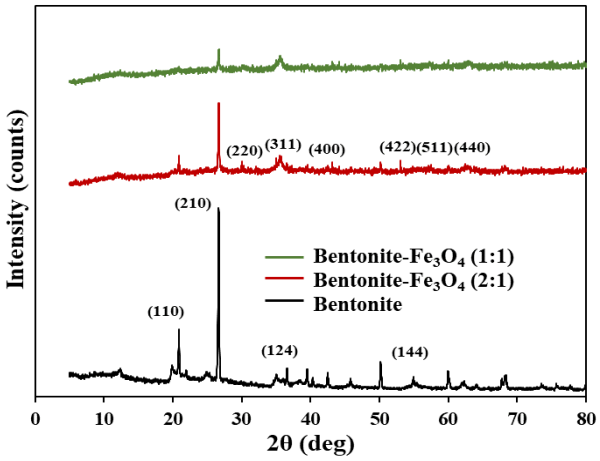

Fig. 1. XRD spectra of bentonite, bentonite-Fe_3O_4 (2:1), and bentonite-Fe_3O_4 (1:1).

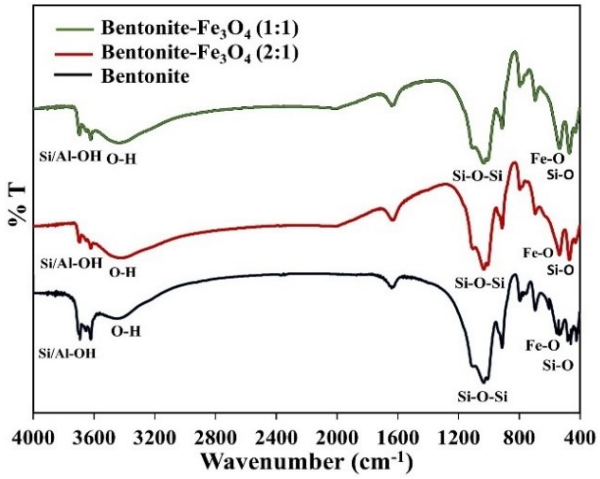

Fig. 2. FTIR spectra of bentonite, bentonite-Fe_3O_4 (2:1) and bentonite-Fe_3O_4 (1:1)

In bentonite, a sharp peak appeared at 912.3 cm^{-1}, which is the Al-O-H group deformation vibration [37]. The peak also appeared with lower intensity in both composites. The peak at wave number 500-600 cm^{-1} indicated the presence of Fe-O bond stretching vibration. In both composites, a sharp peak appeared at the same wave number by 541.6 cm^{-1}, in bentonite observed at 530.4 cm^{-1}. The band as the bond of the Si-O-Si deformation vibration at a wave number of about 460 cm^{-1} appeared in all samples.

Table 1 displays the specific surface area, pore volume, and average pore diameter of bentonite and bentonite-Fe_3O_4 composites. The bentonite surface area was 56.8 m^2/g, smaller than bentonite- Fe_3O_4 (2:1) and bentonite- Fe_3O_4 (1:1) at 86.4 m^2/g and 106.6 m^2/g. The Fe_3O_4 functioned to increase the distance between bentonite layers. In addition to the surface area, the pore volume also increased. Jiang et al. [34] reported the same result where the bentonite-Fe_3O_4-MnO_2 surface area was larger than bentonite. The average pore diameters of bentonite-Fe_3O_4 (2:1) and bentonite-Fe_3O_4 (1:1) were 12.6 nm and 14.8 nm, respectively. As per IUPAC's classification,

mesoporous materials are characterized by an average pore diameter within the range of 2-50 nm

Table 1. Pore parameters of bentonite, bentonite Fe_3O_4 (2:1) and bentonite-Fe_3O_4 (1:1)

Materials	Surface area (m^2/g)	Pore volume (cm^3/g)	Average pore diameter (nm)
Bentonite	56.8	0.124	12.2
Bentonite-Fe_3O_4 (2:1)	86.4	0.248	12.6
Bentonite-Fe_3O_4 (1:1)	106.6	0.782	14.8

The saturation magnetization of the composites was determined at room temperature using a vibrating sample magnetometer, as shown in Figure 3. The saturation magnetization value of bentonite-Fe_3O_4 (1:1) at 69.64 emu/g was found higher than bentonite-Fe_3O_4 (2:1), i.e. 58.93 emu/g. Since bentonite is non-magnetic, it can reduce magnetic properties. The same phenomenon also occurred in the activated carbon-Fe_3O_4 composite in which the saturation magnetization value of the activated carbon-Fe_3O_4 composite increased proportionally with its magnetic content [38]. According to Esakandari et al. [39], particle size also determines magnetic properties. It is directly proportional to magnetic properties due to the decreased domain crystallinity. The saturation magnetization value of bentonite-Fe_3O_4 is classified as superparamagnetic. In this study, the saturation magnetization of bentonite-Fe_3O_4 was found greater than pure Fe_3O_4 synthesized using the sol-gel method, i.e. 47 emu/g [40].

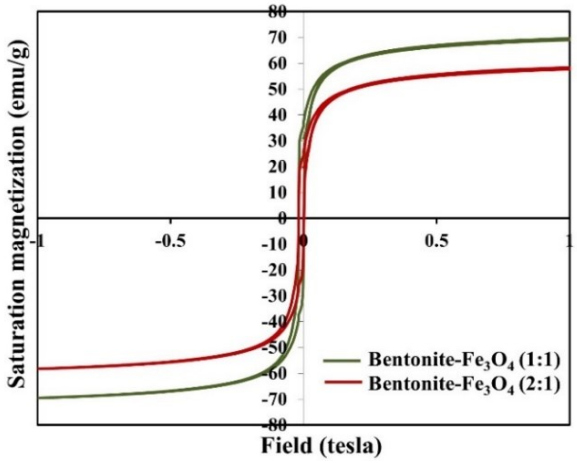

Fig. 3. Saturation magnetization curves of bentonite-Fe_3O_4 (2:1) and bentonite-Fe_3O_4 (1:1).

SEM-EDS analysis determined the morphology and element composition. Figure 4 shows the morphology of bentonite, bentonite-Fe_3O_4 (2:1), and bentonite-Fe_3O_4 (1:1); meanwhile, Table 2 presents the EDS analysis. Bentonite appeared to have layers and was porous, while bentonite-Fe_3O_4 had a denser surface, indicating the presence of Fe_3O_4 entering the bentonite layers. Bentonite had a number of elements including O, Al, Si, K, and Fe with an increase in the percentage of Fe at the bentonite-Fe_3O_4 (2:1) and bentonite-Fe_3O_4 (1:1). Therefore, the composite has been successfully synthesized.

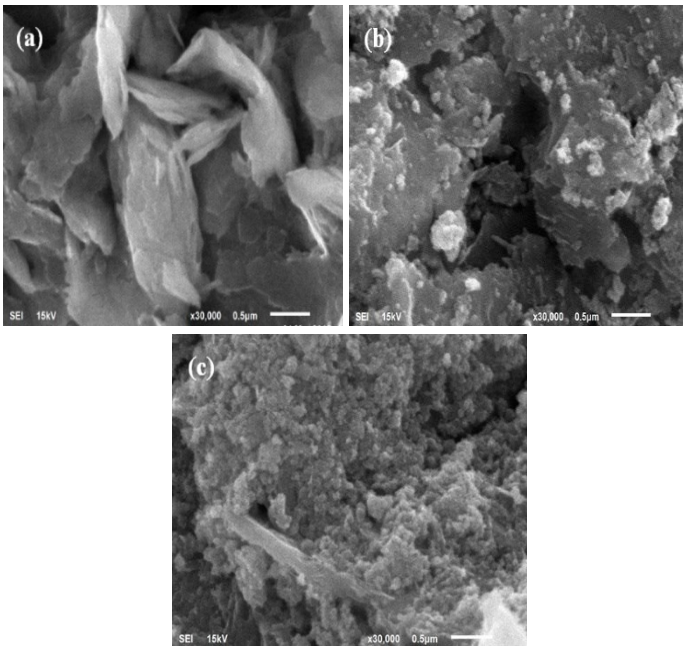

Fig. 4. Morphology of (a) bentonite, bentonite-Fe_3O_4 (2:1) and bentonite-Fe_3O_4 (1:1)

Table 2. Elements composition of bentonite and bentonite-Fe_3O_4 composites.

	Bentonite	Bentonite-Fe_3O_4 (2:1)	Bentonite-Fe_3O_4 (1:1)
O	61.64	62.34	56.58
Al	12.47	5.60	2.48
Si	24.01	12.87	6.82
K	0.58	-	-
Fe	1.30	19.19	34.12

Optical properties are important for material applications in electronic devices and photocatalysts. Figure 5 shows the band gap values of bentonite and bentonite-Fe_3O_4 composites. The bentonite band gap value was 3.70 eV, while the band gap of bentonite-Fe_3O_4 (2:1) and bentonite-Fe_3O_4 (1:1) were 2.62 and 2.25 eV, respectively. These results are similar to Nakhaei et al. [31] where the MnO_2/bentonite band gap was found smaller than bentonite. The decrease in band gap due to ferrite compounds had a reasonably small band gap value of ~2 eV [41].

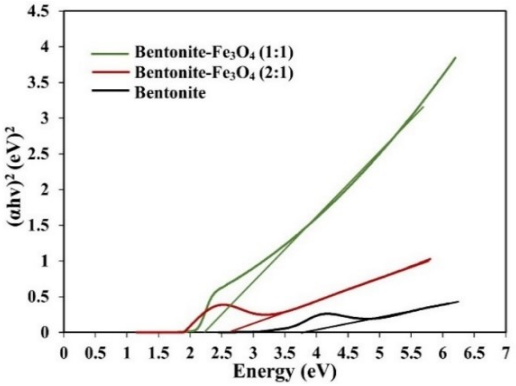

Fig. 5. Band gap of (a) bentonite, (b) bentonite-Fe_3O_4 (2:1), and (c) bentonite-Fe_3O_4 (1:1).

3.2. Photocatalytic degradations of dyes

Bentonite-Fe_3O_4 (1:1) was utilized for the photocatalytic degradation of methylene blue and Congo red dyes due to its larger surface area and smaller band gap compared to bentonite-Fe_3O_4 (2:1). The batch method was utilized to perform the photocatalytic degradation process at ambient temperature. The pH at which the material's charge was neutral was referred to as pH pzc [42]. The pHpzc value of the bentonite-Fe3O4 (1:1) composite was 6.2, as illustrated in Figure 6. The material exhibited a positive charge at pH solution pH pzc and a negative charge at pH solution values above pH pzc. Here, the photocatalytic degradation process was impacted by the charge of both the photocatalyst and the dye.

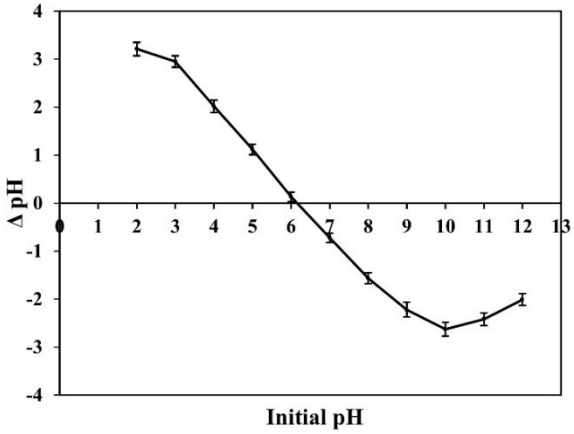

Fig. 6. pH pzc of bentonite-Fe_3O_4 (1:1)

Figure 7(a) presents the impact of pH solution on the degradation efficiency of methylene blue and Congo red dyes. The impact of pH on dye concentration was investigated using a 25 mg/L solution in a 50 mL volume with a catalyst dose of 0.05 g/L and an irradiation duration of 80 minutes. The pH value of 11 was optimal for the photocatalytic degradation of methylene blue dye. Methylene blue is a cationic dye that exhibits greater adsorption efficacy at pH values higher than pHpzc. This is due to the negatively charged nature of bentonite-Fe3O4 (1:1) and the positive charge of the dye.

Another finding revealed that the degradation of methylene blue using Fe2TiO5 was at best at a comparable pH [43]. The optimal pH for the degradation of Congo red dye was 5. Congo red dye exhibited significant solubility in acidic solutions with a pKa value of 4.1 at 25°C, and dissociated into the anion R-SO3- [44]. Less than 5% degradation was observed during the degradation of Congo red dye under alkaline conditions using a poly(p-phenylenediamine)-Fe3O4 in both UV and visible irradiation. Methylene blue dye exhibited over 80% degradation [45].

Figure 7(b) presents the concentration effect on the degradation efficiency. The initial dye concentration was 25-150 mg/L, dose of catalyst 0.05 g/L, pH 11 and 5 for methylene blue and Congo red dyes. The dye concentration is inversely proportional to the degradation efficiency. The availability of active sites on the catalyst surface is restricted in the presence of hydroxyl radicals (•OH), which can be disproportionate to the amount needed for the degradation. Additionally, a large dye concentration blocks the photon's path length to the catalyst, reducing the number of hydroxyl radicals [43].

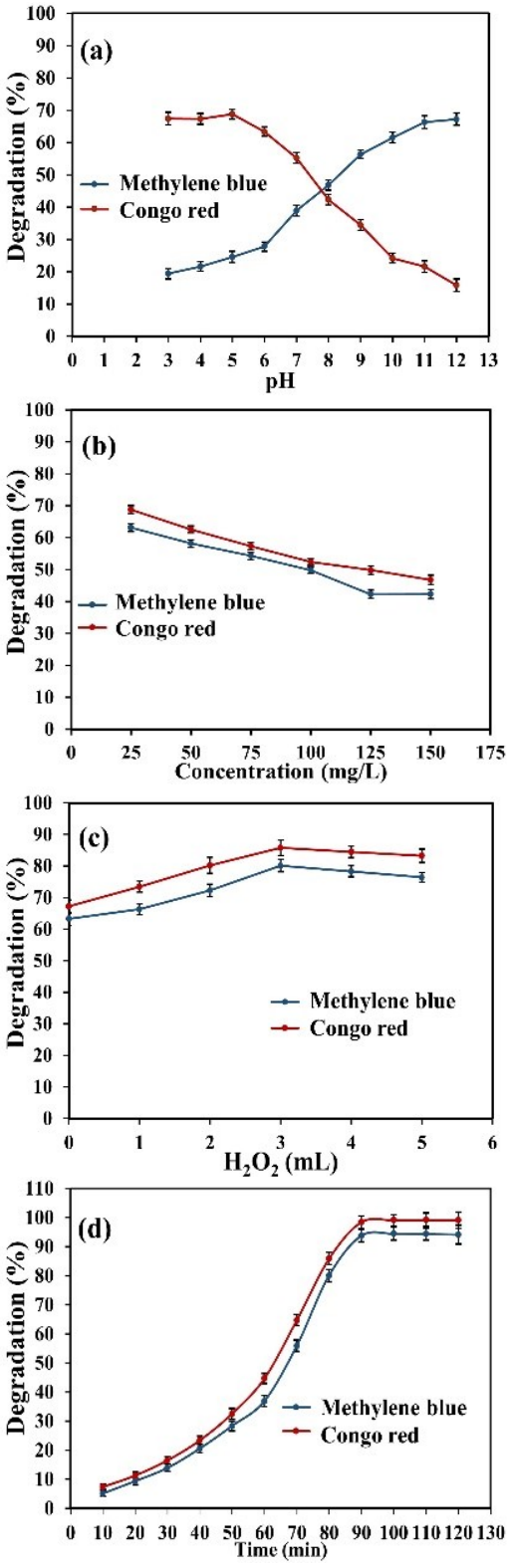

Fig. 7. Effect of (a) pH, (b) initial concentration of dye, (c) volume of H_2O_2, and (d) irradiation time on photocatalytic degradation of methylene blue and Congo red dyes using bentonite-Fe_3O_4 (1:1)

Figure 7(c) shows the effect of H_2O_2 addition on photocatalytic degradation using bentonite-Fe_3O_4 (1:1) with the H_2O_2 (30 %) variation from 1 to 5mL. Photocatalytic degradation can occur without H_2O_2, as photoexcitation

generates electron-hole pairs on the surface of the catalyst. Subsequently, the decomposition of water leads to the generation of hydroxyl radicals (•OH) resulting in the degradation of the dye [46]. The reaction is presented as follows:

$$\text{Bent-Fe}_3\text{O}_4 + hv \rightarrow \text{Bentonite-Fe}_3\text{O}_4(e_{CB}^- + h_{VB}^+) \quad (3)$$

$$\text{H}_2\text{O} + \text{Bent-Fe}_3\text{O}_4(h_{VB}^+) \rightarrow \text{•OH} + \text{H}^+ + \text{Bent-Fe}_3\text{O}_4 \quad (4)$$

$$\text{•OH} + \text{Dye} \rightarrow \text{Degradation product}$$

The hydroxyl radicals' formation significantly accelerated when H_2O_2 was added to the solution, according to the reaction:

$$\text{Bent-Fe}_3\text{O}_4(e_{CB}^-) + \text{H}_2\text{O}_2 \rightarrow \text{OH}^- + \text{•OH} + \text{Bent-Fe}_3\text{O}_4 \quad (5)$$

$$\text{H}_2\text{O}_2 + \text{e}^- \rightarrow \text{•OH} + \text{OH}^- \quad (6)$$

The dye molecules absorb energy and are excited by transferring electrons to Fe(III) to produce Fe(II) when the system is subjected to visible light irradiation, as shown in the following reaction [47]:

$$\text{Dye} + hv \rightarrow \text{Dye}^* \quad (7)$$

$$\text{Dye}^* + \text{Fe(III)} \rightarrow \text{Fe(II)} + \text{Dye}^+\text{•} \quad (8)$$

$$\text{•OH} + \text{Dye/ Dye}^+\text{•} \rightarrow \text{Degradation product} \quad (9)$$

The degradation efficiency of methylene blue and Congo red dyes without H_2O_2 was 63.11 % and 68.78 %, respectively. The highest degradation efficiency with the addition of 3 mL H_2O_2 was 78.23 % and 85.80 % for methylene blue and Congo red dyes. Furthermore, excess H_2O_2 resulted in a reduction in degradation efficiency where it reacted with hydroxyl radicals to produce OOH•, which are the weaker oxidizing agents [48]:

$$\text{H}_2\text{O}_2 + \text{•OH} \rightarrow \text{H}_2\text{O} + \text{OOH•} \quad (10)$$

Figure 7(d) shows the irradiation time effect on degradation efficiency. The pattern of degradation efficiency for both synthetic dyes was the same, increasing at 0-90 minutes. The reaction time can increase by producing more free radicals responsible for degrading dyes [49]. The bentonite-Fe_3O_4 degradation efficiency in Congo red dye was 98.45%, higher than methylene blue dye with 94.34%. The same phenomenon occurred in photocatalytic degradation using Fe_3O_4/ZnO/graphene + H_2O_2 where the degradation efficiency of methylene blue was more significant than Congo red dye [50]. Yang et al. [45] conducted the photocatalytic degradation of 9 types of dyes using poly(p-phenylenediamine)-Fe_3O_4 composite where the percentage for each dye was different. Table 3 presents a comparative analysis of the degradation efficiency of various catalysts in relation to the dyes employed. The degradation efficiency in this study was found better than in some of these studies.

Table 3. The degradation efficiency of some catalysts onto methylene blue dan Congo red dyes

Dye	Catalyst	Initial concentration (mg/L)	Dose (g/L)	pH	Irradiation time (minutes)	Degradation (%)	Ref.
Methylene blue	$CoFe_2O_4 + H_2O_2$	10	0.01	-	140	82.0	[18]
Methylene blue	MnO_2/bentonite	20	0.2	-	120	87.0	[40]
Methylene blue	Fe_2TiO_5	50	0.05	11	250	97.0	[43]
Methylene blue	Brookite-rutile bi-crystalline TiO_2	10	5	-	2160	48.0	[51]
Methylene blue	WO_3	10	0.1	-	60	47.6	[52]
Methylene blue	Bentonite-Fe_3O_4 (1:1)	25	0.05	11	90	94.34	In this study
Congo red	Fenton + Fe_3O_4/ZnO/graphene	40	-	3	120	90.0	[50]
Congo red	$PbTiO_3$	6.97	0.75	6	150	92.0	[53]
Congo red	$CoFe_2O_4$	10	0.35	9	90	92.0	[54]
Congo red	nZVI	220	1.2	4	15	96.0	[55]
Congo red	Ni-TiO_2	10	0.1	2	180	92.31	[56]
Congo red	Bentonite-Fe_3O_4 (1:1)	25	0.05	5	90	98.45	In this study

3.3. Kinetics model of photocatalytic degradation

The photocatalytic degradation kinetics follows the Langmuir-Hinshelwood kinetic model. The constant value can be expressed in a pseudo-first-order equation according to Eq. (11) [18]:

$$\ln \frac{C_0}{C} = kt \quad (11)$$

where C_0 and C are the initial and final concentrations of dye (mg/L), k is the rate constant for pseudo-first-order (min^{-1}), and t is the dye concentration at a certain time (minutes).

Figure 8 depicts the photocatalytic degradation kinetics of

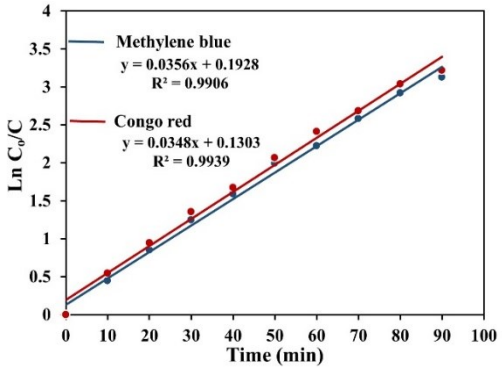

Fig. 8. Kinetic photocatalytic degradation of methylene blue and congo red dyes

the dyes. The dye concentration was 25 mg/L, 50 mL volume, 0.05 g/L catalyst dose, 3 mL H_2O_2, pH 11 and 5. The correlation coefficient (R^2) obtained from the plot $ln\, C_0/C$ versus t was 0.9906 for methylene blue and 0.9939 for Congo red. According to the value of the correlation coefficient, close to 1, the degradation of methylene blue and Congo red dyes followed a pseudo-first-order with k values of 0.0356 min^{-1} and 0.0348 min^{-1}, respectively.

3.4. Reusability of the photocatalyst

Photocatalyst regeneration and reusability are essential for industry. The catalyst should be cheap, applicable, and safe for environment [55]. Catalyst reuse mitigates environmental secondary pollutants. Following photocatalytic degradation, the catalyst was rinsed with deionized water and dried. It underwent the reuse in the photocatalytic degradation procedure. The catalytic degradation process was carried out according to the optimum conditions: the initial concentration of dye 25 mg/L, volume of 50 mL, catalyst dose of 0.05 g/L, 3 mL H_2O_2, and irradiation time of 90 minutes.

Figure 9 shows the degradation efficiency after five experiments. It can be seen that the catalyst had high stability, reusability, and the decrease in the degradation efficiency was insignificant (< less than 5%) for methylene blue and Congo red dyes. The results were better than the photocatalytic degradation of methylene blue dye using Fe_3O_4 + H_2O_2 by 5% after five repetitions [24]. Therefore, bentonite-Fe_3O_4 (1:1) with the H_2O_2 addition under visible irradiation can be stated as an efficient catalyst to remove any contaminants in water, especially dyes. Methylene blue is a synthetic dye commonly utilized within the batik industry [57].

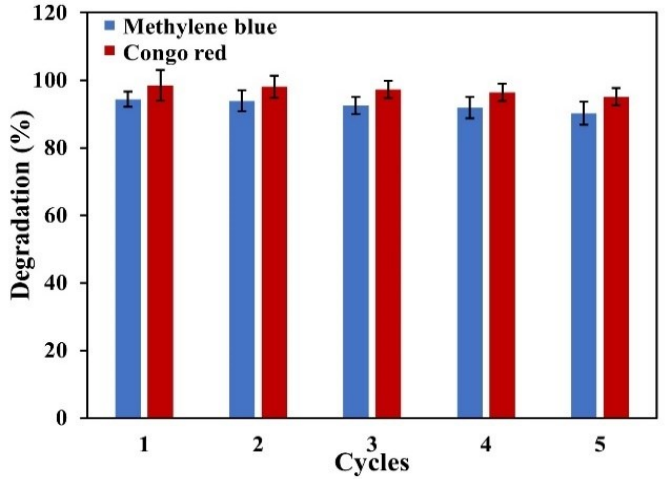

Fig. 9. Reusability of bentonite-Fe_3O_4 (1:1) for photocatalytic degradation of methylene blue and congo red dyes

Total Carbon Analysis (TOC) was employed to assess dye mineralization pre- and post-photocatalytic degradation. Table 4 displays the TOC efficiency of methylene blue at 85.01% and Congo red dyes at 88.99%. These results indicated that the degradation occurred even though the mineralization level was not fully achieved. Similar to another result, the TOC efficiency of photocatalytic degradation using Cu-doped ZnO-MWCNT against rhodamine B dye, phenol, and oxytetracycline (OTC) antibiotics was in the range of 70 to 80% [58].

Table 4. TOC efficiency on photocatalytic degradation of methylene blue and Congo red dyes using bentonite-Fe_3O_4 (1:1)

Dye	TOC (before) (mg/L)	TOC (after) (mg/L)	Efficiency (%)
Methylene blue	41.67	6.25	85.00
Congo red	62.87	6.92	88.99

4. Conclusion

Bentonite-Fe_3O_4 magnetic has been synthesized by the co-precipitation method. Bentonite-Fe_3O_4 with a mass ratio of 1:1 showed a larger surface area and saturation magnetization than bentonite-Fe_3O_4 with a ratio of 2:1, while the band gap of bentonite-Fe_3O_4 (1:1) was smaller than bentonite-Fe_3O_4 (2:1). The bentonite-Fe_3O_4 (1:1) is superparamagnetic and this property is the advantage of a catalyst. After the photocatalytic degradation process, the catalyst can be quickly separated from the solution using a permanent magnet. The application of bentonite-Fe_3O_4 (1:1) for photocatalytic degradation to methylene blue and Congo red dyes showed a higher degradation efficiency to Congo red at 98.45% compared to methylene blue at 94.34%. The bentonite-Fe_3O_4 (1:1) can potentially be used for wastewater treatment, especially those containing industry dyes. The five-time reusability of the bentonite-Fe_3O_4 (1:1) for photocatalytic degradation, which has a high degradation percentage, showed good performance and stability catalyst.

Acknowledgement

The author acknowledges the financial assistance provided by the "Unggulan Profesi" Program of the Public Service Agency of Universitas Sriwijaya in 2022 under SP DIPA-023.17.2.677515/2022 on December 13, 2021. On April 28, 2022, in compliance with Rector's Decree No. 0111/UN9.3.1/SK/2022.

References

1. L. Wang, J. Li, Y. Wang, L. Zhao, Q. Jiang, *Adsorption capability for congo red on nanocrystalline MFe_2O_4 (M = Mn, Fe, Co, Ni) spinel ferrites*, J. Chem. Eng. 72-79 (2012) 181-182.
2. A. He, R. Lu, Y. Wang, J. Xiang, Y. Li, D. He, *Adsorption Characteristic of Congo Red Onto Magnetic $MgFe_2O_4$ Nanoparticles Prepared via the Solution and Gel Calcination Process*, J. Nanosci. Nanotechnol. 17 (2017) 3967-3974.
3. J.T. Adeleke, Theivasanthi, M. Thiruppathi, M. Swaminathan, T. Akomolafe, A.B. Alabi, *Photocatalytic degradation of methylene blue by $ZnO/NiFe_2O_4$ nanoparticles*, Appl. Surf. Sci. 455 (2018) 195-200.
4. H. Hanafy, *Adsorption of methylene blue and bright blue dyes on bayleaf capertree pods powder: understanding the adsorption mechanism by a theoretical study*, J. Mol. Liq. 332 (2021) 1-5.
5. M. Iram, C. Guo, Y. Guan, A. Ishfag, H. Liu, *Adsorption and magnetic removal of neutral red dye from aqueous solution using Fe_3O_4 hollow nanospheres,* J. Hazard. Mater. 181 (2010) 1039-1050.
6. Y. Li, A. Meas, S. Shan, R. Yang, X. Gai, *Production and optimization of bamboo hydrochars for adsorption of congo red and 2-naphthol*, Bioresour. Technol. 207 (2016) 379-386.
7. C. K. Mangat, S. Kaur, *Efficient removal and separation of anionic dyes*

from aqueous medium by the application of reverse micelles of cationic surfactants, Desalin. Water Treat. 52 (2014) 3555–3563.

8. Y. Song, et al., *The feasibility of UF-RO integrated membrane system combined with coagulation/flocculation for hairwork dyeing effluent reclamation*, Sci. Total Environ. 691 (2019) 45-54.
9. M.S. Anantha, S. Olivera, C. Hu, B.K. Jayanna, N. Reddy, *Comparison of the photocatalytic, adsorption and electrochemical methods for the removal of cationic dyes from aqueous solutions*, Environ. Technol. Innov. 17 (2020), 1-20.
10. J. Li, et al., *Improved water permeability and structural stability in a polysulfone-grafted graphene oxide composite membrane used for dye separation*, J. Membr. Sci. 595 (2020) 1-11.
11. K.H.H. Aziz et al., *Comparative study on 2,4-dichlorophenoxyacetic acid and 2,4-dichlorophenol removal from aqueous solutions via ozonation, photocatalysis and non-thermal plasma using a planar falling film reactor*, J. Hazard. Mater. 343 (2018) 107-115.
12. A. Rafig et al., *Photocatalytic degradation of dyes using semiconductor photocatalysts to clean industrial water pollution*, J. Ind. Eng. Chem. 97 (2021) 111-128.
13. N. Fessi et al., *Surface and electronic features of fluorinated TiO_2 and their influence on the photocatalytic degradation of 1-Methylnaphalene,* J. Phys. Chem. C 124 (2020) 11456-11468.
14. M.K.H.M. Hanif, N.A. Sapawe, *Short review on photocatalytic toward dye degradation*, Mater. Today 31 (2020) A42-A47.
15. Z. Hu, J. Fan, K. Zhang, N. Yu, J. Wang, *Pharmaceutical removal by novel nanoscale photocatalyst Bi_4VO_8Cl: influencing factors, kinetics, and mechanism*, Ind. Eng. Chem. Res. 53 (2014) 14623-14632.
16. D. Guin, B. Baruwati, S.V. Manorama, *A simple chemical synthesis of nanocrystalline AFe_2O_4 (A = Fe, Ni, Zn): an efficient catalyst for selective oxidation of styrene*, J. Mol. Catal. A: Chem. 242 (2005) 26-31.
17. Z. Li, X. Lai, H. Wang, D. Mao, C. Xing, D. Wang, *General synthesis of homogeneous hollow core-shell ferrite microspheres*, J. Phys. Chem. C. 113 (2009) 2792-2797.
18. K. Maaz, A. Mumtaz, S.K. Hasanain, A. Ceylan, *Synthesis and magnetic properties of cobalt ferrite ($CoFe_2O_4$) nanoparticles prepared by wet chemical route*, J. Magn. Magn. Mater. 308 (2007) 289-295.
19. A. Kalam et al., *Modified solvothermal synthesis of cobalt ferrite ($CoFe_2O_4$) magnetic nanoparticles photocatalysts for degradation of methylene blue with H_2O_2/visible light*, Results Phys. 8 (2018) 1046-1053.
20. R. Dom, R. Subasri, K. Radha, P.H. Borse, *Synthesis of solar active nanocrystalline ferrite, MFe_2O_4 (M: Ca, Zn, mg) photocatalyst by microwave irradiation*, Solid State Commun. 151 (2011) 470-473.
21. I.J. Ani, U.G. Akpan, M.A. Olutoye, B.H. Hameed, *Photocatalytic degradation of pollutants in petroleum refinery wastewater by TiO_2- and ZnO-based photocatalysts: recent development*, J. Clean. Prod. 205 (2018) 930-954.
22. T.P. Oliveira et al., *Synthesis and photocatalytic investigation of $ZnFe_2O_4$ in the degradation of organic dyes under visible light*, J. Mater. Res. Technol. 9 (2020) 15001-15015.
23. C. B. Ong, L. Y. Ng, A. W. Mohammad, A review of ZnO nanoparticles as solar photocatalysis: synthesis, mechanism and applications, Renew. Sust. Energ. Rev. 81 (2018) 536-551.
24. P.L. Hariani M. Said, A. Rachmat, F. Riyanti, H.C. Pratiwi, W.T. Rizki, *Preparation of $NiFe_2O_4$ nanoparticles by solution combustion method as photocatalyst of congo red*, Bull. Chem. React. Eng. 16 (2021) 481-490.
25. J. Zhang, S. Fan, B. Lu, Q. Cai, J. Zhao, S. Zang, *Photodegradation of naphthalene over Fe_3O_4 under visible light irradiation*, R. Soc. Open. Sci. 6 (2018) 1-15.
26. C. Hung, C. Chen, Y. Jhuang, C. Dong, *Fe_3O_4 magnetic nanoparticles: characterization and performance exemplified by the degradation of methylene blue in the presence of persulfate*, J. Adv. Oxid. Technol. 19 (2016) 43-51.
27. L. Yan, S. Li, H. Yu, R. Shan, B. Du, T. Liu, *Facile solvothermal synthesis of Fe_3O_4/bentonite for efficient removal of heavy metals from aqueous solution*, Powder Technol 301 (2016) 632-640.
28. D. Cho, B. Jeon, C. Chon, F.W. Schwartz, Y. Jeong H. Song, *Magnetic chitosan composite for adsorption of cationic and anionic dyes in aqueous solution*, J Ind Eng Chem 28 (2015) 60-66.
29. T.Y. Ying, A.A.A. Raman, Bello, M.M.; Buthiyappan, A. *Magnetic graphene oxide-biomass activated carbon composite for dye removal*, Korean J. Chem. Eng. 37 (2020) 1-16.
30. C. Modrogan, et al., *Modified composite based on magnetite and polyvinyl alcohol: synthesis, characterization, and degradation, studies of the methyl orange dye from synthetic wastewater*, Polymers 13 (2021) 1-13.
31. M. Nakhaei, Z. Barzgari, S.S. Mohammadi, A. Ghazizadeh, *Preparation of MnO_2/bentonite nanocomposite with enhanced photocatalytic activity under sunlight irradiation*, Res. Chem. Intermed. 45 (2019) 4995-5005.
32. A.A. Taha, M.A. Shreadah, A.M. Ahmed, H.F. Heiba, *Multi-component adsorption of Pb(II), Cd(II), and Ni(II) onto Egyptian Na-activated bentonite; equilibrium, kinetics, thermodynamics, and application for seawater desalination*, J. Environ. Chem. Eng. 4 (2016) 1166-1180.
33. R. Zhu, Q. Chen, Q. Zhou, Y. Xi, J. Zhu, H. He, *Adsorbents based on montmorillonite for contaminant removal from water: A review*, Appl. Clay Sci. 123 (2016) 239-258.
34. L. Jiang, Q. Ye, J Chen, Z. Chen, Y. Gu, *Preparation of magnetically recoverable bentonite–Fe_3O_4–MnO_2 composite particles for Cd(II) removal from aqueous solutions*, J. Colloid Interface Sci. 513 (2018) 748-759.
35. J. Jiang, J. Zou, L. Zhu, L. Huang, H. Jiang, Y. Zhang, Degradation of methylene blue with H2O2 activated by peroxidase-like Fe_3O_4 magnetic nanoparticles, J. Nanosci. Nanotechnol. 11 (2011) 4793-4799.
36. Y. Fan, F. Zhang, Y. Feng, *An effective adsorbent developed from municipal solid waste and coal co-combustion ash for As(V) removal from aqueous solution*, J. Hazard. Mater. 59 (2008) 313-318.
37. M. Fayazi, M.A. Taher, D. Afzali, A. Mostafavi, *Fe_3O_4 and MnO_2 assembled on halloysite nanotubes: A highly efficient solid-phase extractant for electrochemical detection of mercury(II) ions*, Sens. Actuators B Chem. 228 (2016) 1-9.
38. R. Juang et al., *Synthesis of magnetic Fe_3O_4/activated carbon nanocomposites with high surface area as recoverable adsorbents,* J. Taiwan Inst. Chem. Eng. 90 (2018) 51-60.
39. M.J. Eskandari, I. Hasanzadeh, *Size-controlled synthesis of Fe_3O_4 magnetic nanoparticles via an alternating magnetic field and ultrasonic-assisted chemical co-precipitation,* J. Mater. Sci. Eng. B. 266 (2021) 1-10.
40. O.M. Lemine, *Sol–gel synthesis of 8 nm magnetite (Fe_3O_4) nanoparticles and their magnetic properties*, Superlattices Microstruct. 52 (2012) 793-799.
41. E. Casbeer, V.K. Sharma, X. Li, *Synthesis and photocatalytic activity of ferrites under visible light: a review*, Sep. Purif. Technol. 87 (2012) 1-14.
42. M.A.S. Amulya, H.P. Nagawarupa, M.R.A. Kumar, C.R. Ravikumar, S.C. Prashanta, K.B. Kususma, *Sonochemical synthesis of $NiFe_2O_4$ nanoparticles: characterization and their photocatalytic and electrochemical applications*. Appl. Surf. Sci. 1 (2020) 1-10.
43. Z.Z. Vasiljevic et al. *Photocatalytic degradation of methylene blue under natural sunlight using iron titanate nanoparticles prepared by a modified sol–gel method,* R. Soc. Open Sci. 7 (2020) 1-14.
44. R. Lafi, I. Montasser, A. Hafiane, *Adsorption of congo red dye from*

aqueous solutions by prepared activated carbon with oxygen-containing functional groups and its regeneration, Adsorp. Sci. Technol. 37 (2018) 160-181.

45. S. Yang, C. Ye, X. Song, L. He, F. Liao, *Theoretical calculation based synthesis of a poly(p-phenylenediamine)–Fe_3O_4 composite: a magnetically recyclable photocatalyst with high selectivity for acid dyes*, RSC Adv. 4 (2014) 54810-54818.
46. R.V. Solomon, I.S. Lydia, J.P. Merlin, P. Venuvalingam, *Enhanced photocatalytic degradation of azo dyes using nano Fe_3O_4*, J. Iran. Chem. Soc. 9 (2012) 101-109.
47. Y. Gao, Y. Wang, H. Zhang, *Removal of rhodamine B with Fe-supported bentonite as heterogeneous photo-Fenton catalyst under visible irradiation*, Appl. Catal. 178 (2015) 29-36.
48. A. Mohammadzadeh, M. Khoshghadam-Pireyousefan, B. Shokrianfard-Ravasjan, H. Azadbeh, M. Dibazar, A. Mostafaei, *Synergetic photocatalytic effect of high purity ZnO pod shaped nanostructures with H_2O_2 on methylene blue dye degradation,* J. Alloys Compd. 845 (2020) 1-11.
49. A. Pourzad, H.R. Sobhi, M. Behbahani, A. Esrafili, R.R. Kalantary, M. Kermani, *Efficient visible Light-induced photocatalytic removal of paraquat using N-doped TiO_2@SiO_2@Fe_3O_4 nanocomposite*, J. Mol. Liq 299 (2020) 1-7.
50. R. Saleh, A. Taufik, *Degradation of methylene blue and congo-red dyes using Fenton, photo-Fenton, sono-Fenton, and sonophoto-Fenton methods in the presence of iron (II,III) oxide/zinc oxide/graphene (Fe_3O_4/ZnO/graphene) composites*, Sep. Purif. Technol. 210 (2019) 563-573.
51. M.G. Kim, J.E. Lee, K.S. Kim, J.M. Kang, J.H. Lee, K.H. Kim, S.G. Lee, *Photocatalytic degradation of methylene blue under UV and visible light by brookite–rutile bi-crystalline phase of TiO_2*, New J. Chem. 45 (2021) 3485-3497.
52. X. Yin, L. Liu, F. Ai, *Enhanced photocatalytic degradation of methylene blue by WO_3 nanoparticles under NIR light irradiation*, Front. Chem. 9 (2021) 1-9.
53. U.O. Bhagwat, J.J. Wu, A.M. Asiri, S. Anandan, *Photocatalytic degradation of congo red Using $PbTiO_3$ nanorods synthesized via a sonochemical approach,* Chem. Eur. J. 3 (2018) 11851-11858.
54. N. Ali et al., *Photocatalytic degradation of congo red dye from aqueous environment using Cobalt Ferrite nanostructures*: *development, characterization, and photocatalytic performance,* Water Air Soil Pollut. 231 (2020) 1-16.
55. A.K. Jha, S. Chakraborty, *Photocatalytic degradation of congo red under UV irradiation by zero valent iron nano particles (nZVI) synthesized using Shorea robusta (Sal) leaf extract*, Water Sci. Technol. 82 (2020) 2491-2502.
56. K. Indira, et al., *Photocatalytic degradation of congo red dye using nickel–titanium dioxide nanoflakes synthesized by Mukia madrasapatna leaf extract*, Environ. Res. 202 (2021) 1-8.
57. M. Rahmayanti, A. Yahdiyani, I.F. Afifah, *Eco-friendly synthesis of magnetite based on tea dregs (Fe_3O_4-TD) for methylene blue adsorbent from simulation waste*, Commun. Sci. Technol. 7 (2022) 119-126.
58. D. Toloman et al., *Visible-light-driven photocatalytic degradation of different organic pollutants using Cu doped ZnO-MWCNT nanocomposites*, J. Alloys Compd. 866 (2021) 1-14.